Journal of Power Sources 195 (2010) 5587–5595

Contents lists available at ScienceDirect

Journal of Power Sources

journal homepage: www.elsevier.com/locate/jpowsour

Low temperature pyrolyzed cobalt tetramethoxy phenylporphyrin catalyst and its applications as an improved catalyst for metal air batteries

Aaron Li Zhu, Haijiang Wang*, Wei Qu, Xiaoxia Li, Zoe Jong, Hui Li

Institute for Fuel Cell Innovation, National Research Council Canada, 4250 Wesbrook Mall, Vancouver, B.C. V6T 1W5, Canada

ARTICLE INFO

Article history:
Received 5 February 2010
Received in revised form 5 March 2010
Accepted 8 March 2010
Available online 12 March 2010

Keywords:
Alkaline electrolyte
Catalyst
CoTMPP/C
Metal–air battery
Oxygen reduction reaction (ORR)

ABSTRACT

As an alternative catalyst to replace the expensive platinum-based catalysts for oxygen reduction reaction (ORR) in both proton exchange membrane (PEM) fuel cells and metal–air batteries, tetra methoxyphenyl porphyrin cobalt complex, CoTMPP, has drawn much attention in the areas of ORR catalyst synthesis and characterization. In the present work, CoTMPP is investigated at varying temperatures of pyrolysis, ranging from 410 to 810 °C, to determine the optimal temperature of pyrolysis to produce catalysts with desirable properties. Carbon supported pyrolyzed CoTMPP catalyst (CoTMPP/C) was assessed using X-ray diffraction and Raman, a number of varied electrochemical tests, as well as a single cell test. Through these, it has been found that the CoTMPP/C, pyrolyzed at 410 °C, demonstrates superior catalytic activity towards ORR, and has a higher fuel cell performance than the catalysts pyrolyzed at 800 °C, the industry standard pyrolysis temperature. This paper also utilizes scanning auger microscopy (SAM) to accredit the origin of the increased activity to the bond N–C(O), which plays a major role in catalysis and is decomposed at higher temperatures.

1. Introduction

The sluggish kinetics of ORR has resulted in ORR catalysis being the main focus in the areas of catalyst synthesis and characterization for both PEM fuel cells and metal–air batteries [1,2]. One of the main challenges remaining is the discovery of inexpensive and stable catalysts with superior catalytic performance in accelerating the ORR. As of current, the catalysts in fuel cell prototypes are comprised of platinum or platinum-based alloyed nanoparticles supported on carbon black (Pt/C); however, high cost and shortage of natural sources of Pt constraint further commercialization [3]. One area of research has focused on the development of non-precious metal-based materials as alternative catalysts; yet, to be feasible their activity indices would have to approach those of traditional Pt-based catalysts. Very recently, Dodelet and co-workers [4] have reported a breakthrough in the performance of ORR catalysts, based on non-precious metals, which exhibit a premier crystal structure resembling the core structure of the CoTMPP. In a preliminary test with a proton exchange membrane (PEM), a very striking volumetric activity (99 A cm^{-3}) was found, suggesting that the catalyst had reached the same functional level as that of Pt (Gore, USA). Albeit many studies have already been conducted on CoTMPP in acidic PEM fuel cells [5], this new development has inspired a systematic re-inspection of CoTMPP for its applications in alkaline fuel cells and metal–air batteries.

This report will provide an in-depth assessment on CoTMPP in an effort to evaluate its applications in an alkaline environment. In particular, the effect of pyrolysis temperature of the CoTMPP/C catalyst on its catalytic activity towards ORR was studied using various techniques. Simultaneous differential scanning calorimetry with thermogravimetric analysis (DSC–TGA) was used to investigate the pyrolysis of CoTMPP at differing temperatures. The crystalline state and the interaction between CoTMPP and the carbon support following heat treatment were assessed by X-ray diffraction (XRD) followed by an examination with Micro-Raman. The electrochemical performance, electron transfer number during ORR and the durability of the optimized CoTMPP/C catalysts after selective decomposition were measured and then evaluated via linear scan voltammetry (LSV), cyclic voltammetry (CV), rotating disk electrode (RDE) and the rotating ring disk electrode (RRDE) techniques, respectively. The chemical states of the Co–N bond and Co–N–C bonds of the CoTMPP/C catalysts were measured by X-ray photoelectron spectroscopy (XPS) and scanning Auger microscopy (SAM). The results of alkaline single fuel cell tests for the selected CoTMPP/C catalysts are also provided in this report.

2. Experimental

2.1. Preparation of the Vulcan carbon supported CoTMPP catalyst (CoTMPP/C)

200 mg of Vulcan XC72 carbon (cabot) containing *ca.* 3 wt% of cobalt tetramethoxy-phenylporphyrin (CoTMPP, Sigma–Aldrich) was impregnated in 25 mL of isopropanol (Alfa Aesar) for 12 h in

* Corresponding author. Tel.: +1 604 221 3087; fax: +1 604 221 3001.
E-mail address: haijiang.wang@nrc.gc.ca (H. Wang).

0378-7753/$ – see front matter.
doi:10.1016/j.jpowsour.2010.03.015

a sealed clean glass container. The contents were then amalgamated using a rotating ultrasonic probe processor (Cole Parma) for 30 min, followed by 1 h of conventional ultrasonication to ensure complete suspension and homogenization. Subsequently the resulting slurry was gradually dried in air, then placed in a continuous high purity (99.99%, 5 $dm^3\,min^{-1}$) N_2 flow furnace (Thermcraft) utilizing a 5 °C min^{-1} heating and cooling rate for heat treatment at 410, 440, 600, 700, 800 and 810 °C, respectively. Each temperature was held for 30 min upon the arrival of the designated temperatures as indicated by the furnace sensor. The error in the temperature of the furnace sensor was measured at different temperatures and were found to be: ±2 °C at a low temperature scale (<300 °C), ±5 °C at a medium temperature scale (400–700 °C) and ±10 °C at a high temperature scale (>750 °C).

2.2. Electrode preparation and electrochemical measurements in a three-electrode cell

A catalyst ink was prepared by soaking 200 mg of dry CoTMPP/C powder in 10 mL ethanol (Sigma–Aldrich) and ultrasonicating the mixture for 30 min. After ultrsonication, 20 μL of well-mixed CoTMPP/C ink was uniformly applied onto the glassy carbon (GC) disk surfaces of a RDE (Pine) and a RRDE (Pine) with geometric disk areas of 0.164 and 0.247 cm^2, respectively, yielding a CoTMPP loading of 0.07 mg cm^{-2} and 0.05 mg cm^{-2}, respectively. This application was followed by a pipetting of 4 μL of 1% Nafion, prepared by a dilution from the commercial 5% Nafion (Du Pont) with isopropanol, on top of the catalyst ink. The coated electrodes were then left to dry in air under the light of a 20 W desk lamp for at least 1 h. To ensure complete coverage and coating layer uniformity the prepared electrode was frequently assessed using a digital optical microscope (ImagingSource). Occasionally, the thickness of the coating layer was evaluated using Kolb's method [6] to guarantee that the Nafion layer resistance was negligible and that the catalyst layer was thin enough to ensure the geometric electrode area could be used directly in calculations for investigating catalyst ORR mechanisms.

For electrochemical measurements, LSV, CV, and dynamic polarization techniques on the RDE and RRDE were employed. The collection efficiency of the RRDE was calibrated to 0.39 by employing a 10 mM $K_3[Fe(CN)_6]$ (Fischer) solution in nitrogen saturated 0.1 M KOH (Alfa Aesar) [7]. All the electrochemical measurements were performed using a jacketed three-compartment electrochemical cell, an MSR rotator (Pine Instruments) and a computerized Solartron 1408 multiple channel potentiostate (Ametek). 1.5 cm × 1 cm Pt gauze and a commercial Hg/HgO electrode in 6 M KOH (Pine, 0.060 V *vs.* NHE) were used as the counter electrode and reference electrode, respectively, and O_2-free and O_2-saturated 6 M KOH (Alfa Aesar) solutions were used as electrolytes. Prior to each experiment, the GC electrode was first cleaned using ethanol and distilled water (Milli-Q, 18 MΩ cm), and then ultrasonicated for 2 min. Subsequently, the cleanliness of the electrolyte and GC electrode was assessed by comparing the background cyclic voltammogram against the standard obtained from a clean and new commercial GC analytical electrode (Pine).

2.3. Single cell test

The single cell was a unit designed in-house with a self-breathing architecture. The air cathode consisted of a gas diffusion layer (GDL) and a catalyst layer. The GDL was acquired from SGL Company (Germany) with 20 wt% PTFE, and the catalyst was applied on the GDL by means of the spray method resulting in an active area of 18 cm^2. The catalyst loadings for CoTMPP/C pyrolyzed at 410 and 800 °C were only 0.08 and 0.09 mg cm^{-2} in an effort to find the difference in catalytic activities of both catalysts. The catalyst spray was carried out via a homemade sprayer constructed from a Vextra X-Y table (model PK266-03A-P1, Oriental Motor Inc., Japan), an airbrush set (Badger, USA) and self-modified software. Expanded copper mesh was then clad to the edges of the air cathode to collect the current. A Zn sheet (Fisher) was used as an anode, and the electrolyte used in the single cell was the same as that used for the half cell electrochemical measurements. The test was carried out using a fuel cell test station (FuelCon, Germany).

2.4. Instrumental characterization of the catalysts

The pyrolysis of CoTMPP/C at differing temperatures, ranging from room temperature to 1000 °C in N_2, was monitored by a simultaneous differential scanning calorimetry and thermogravimetric analysis system (DSC–TGA, TA Instruments). The chemical state of CoTMPP/C was examined by X-ray photoelectron spectroscopy (XPS) using a Leybold MAX200 system (Leybold, Germany) operated with a Mg Kα source (1253.6 eV) at 10 kV, 20 mA, and with pass energies of 192 and 48 eV for obtaining the screening and high-resolution spectra, respectively. The analytical chamber was held at 2×10^{-9} mbar and all binding energies were referenced to the adventitious hydrocarbon C 1s peak at 285.0 eV. To study the local micro-regions of the catalyst powder surface, Auger spectra, scanning electron micrographs and backscattered electron (BSE) images were obtained using a SAM Microlab 350 system (Thermo Electron Corp) equipped with a field emission source (10 keV, 3.5 nA) and hemispherical energy analyzer. The crystalline state of CoTMPP/C was assessed by X-ray diffraction (XRD). The data were collected with a Bruker D8 Advance (Bruker) diffractometer (Cu K-α1 source) over the range of 5–90° 2–2θ with a scanning rate of 0.02° s^{-1}; before each measurement the diffractometer was calibrated using the Si wafer provided by the manufacturer. Each XRD pattern was obtained through cyclic scanning for a 12-h period. The interaction between CoTMPP and carbon support was measured by Micro-Raman. The spectra were acquired via an XploRA Spectrometer (HORIBA Jobin Yvon) with a 532 nm laser source (the laser power with no attenuation was 15.4 mW) and a 100× objective (detective spot size was 1 μm). It is of interest to note here that CoTMPP is very sensitive to laser exposure and laser-induced structure conversion is a straightforward method to yield new sharp peaks in XRD. Therefore, fine-tuning of the laser power must be carried out before all measurements. Furthermore, since CoTMPP is heat sensitive and laser-induced conversions are probable, other laser sources were not selected and the laser filter was set to only 10%.

3. Results and discussion

3.1. Pyrolysis process analysis

To optimize heat treatment temperatures used to obtain the best catalytic performance from CoTMPP, an understanding of the pyrolysis process was necessary. Therefore, the thermal decomposition of CoTMPP was measured, and the results served as guidance for future sample preparation and characterizations. Fig. 1 reveals that the pyrolysis process initiates at 400 °C. The first substantial change in CoTMPP structure occurs in the decomposition stage I, when the pyrolysis temperature reaches 409 °C, corresponding to fast molecular structure variation and bond shrinkage. The second change occurs at 440 °C where the reaction speed of stage II slows in comparison to stage I, suggesting an endothermic reaction of the solid structure melting. Stage II ends at about 600 °C with the major reactions correlating to the structure-breaking fragmentation of the methoxyphenyl groups [8]. No dramatic changes occur

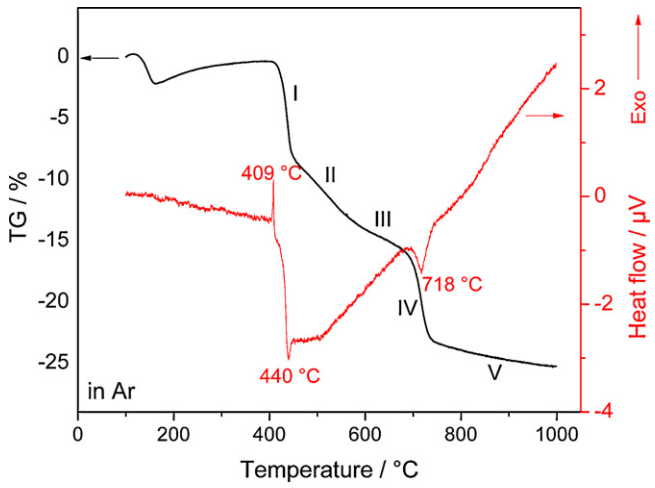

Fig. 1. Differential scanning calorimetric measurements combined with thermogravimetric analysis (DSC–TGA) for CoTMPP. The temperature increasing and decreasing rate is 5 °C min^{-1}. The measurement was performed in Ar flow environment.

in stage III, which may be explained by the continuation and completion of the prior decomposition reactions. In stage IV, a strong alteration of the curve occurred at 718 °C, which is thought to stem from a CO_2 release at the carbonyl groups. No significant transformation in the CoTMPP molecular decomposition can be found in the stage V as the original CoTMPP molecule has been pyrolyzed into fragments and moieties; however, CoTMPP does undergo continuous decomposition with the steadily increasing temperature, with the weight loss of CoTMPP reaching a fairly high level at 800 °C.

3.2. Post-pyrolysis analysis with XRD

High-resolution XRD patterns (Fig. 2) were obtained from the Vulcan XC72 carbon support, commercial CoTMPP (Alfa Aesar), CoTMPP absorbed on Vulcan carbon via isopropanol, and CoTMPP/C pyrolyzed at 410, 440, 600, 700, 800 and 810 °C, respectively. It is hard to differentiate between the XRD patterns of carbon, and CoTMPP/C catalysts heat-treated respectively at 440, 600, 700, 800 and 810 °C since the peaks representing Vulcan carbon dominate the patterns. However, careful measurement reveals that the full width at half maximum (FWHM) of the principal carbon peak at *ca.* 24° (2θ) varies in the XRD patterns of CoTMPP/C pyrolyzed at

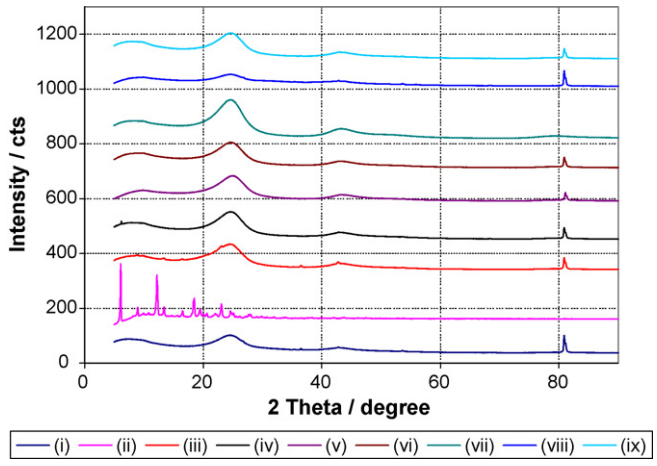

Fig. 2. X-ray diffractograms of (i) Vulcan XC72 carbon, (ii) commercial CoTMPP, (iii) CoTMPP absorbed on carbon, and CoTMPP/C pyrolyzed at (iv) 410 °C, (v) 440 °C, (vi) 600 °C, (vii) 710 °C, (viii) 800 °C, (ix) 810 °C.

different temperatures. Since the carbon cannot vary its own size at such a low temperature range, this suggests the presence of an interaction between the carbon and CoTMPP moieties, and that the CoTMPP portions have been buried in the carbon matrix during the pyrolysis process [9]. The XRD pattern of CoTMPP/C pyrolyzed at 410 °C (iv) demonstrates an obvious additional peak at 6.2° when compared with the catalysts pyrolyzed at the remaining temperatures. This additional peak overlaps perfectly with the peak of CoTMPP (ii) at the same 2θ location and does not appear in the patterns of CoTMPP pyrolyzed at the other temperatures or in the pattern for CoTMPP absorbed on carbon before performing pyrolysis. This finding suggests that the species represented by this peak likely plays an important role in the unique catalytic performance of CoTMPP/C catalyst pyrolyzed at 410 °C.

3.3. Raman analysis for the CoTMPP/C catalysts

Since large molecular changes during pyrolysis are reflected by changes in the Raman spectrum, Raman analysis is an important tool to assess CoTMPP/C as a catalyst at varying temperatures. Furthermore, the Raman peaks or peak shifts may also represent the decomposed products, which are directly related to catalysis. More importantly, it has been proven that some of the carbon layers of the support strongly link to the Co–N_x catalytic moieties. As a result, the C becomes actively involved in ORR catalysis and the current density of the ORR dramatically increases [4]. Therefore, Raman analysis is utilized as it is powerful enough to directly detect the effect on carbon due to the interaction between the catalyst and the carbon support. Fig. 3 shows the Raman spectra of Vulcan XC-72 carbon, CoTMPP, CoTMPP absorbed on Vulcan carbon before heat treatment, and CoTMPP/C after pyrolysis at 410, 440, 600, 700, 800 and 810 °C, respectively. To obtain each spectrum, at least 6 dif-

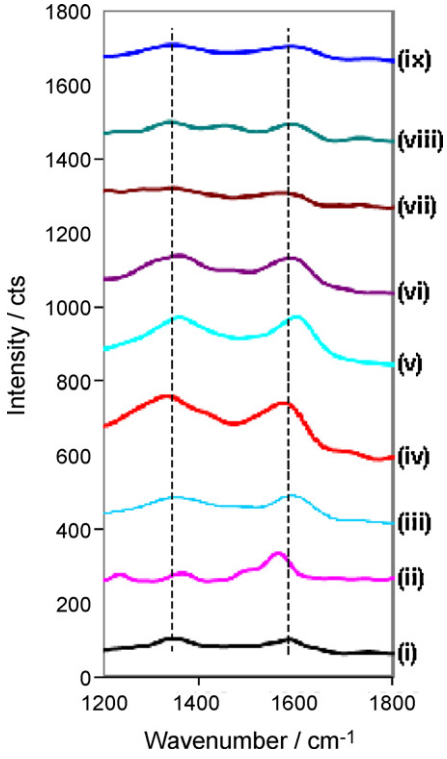

Fig. 3. Raman spectra for the samples pyrolyzed at the different temperatures, (i) Vulcan XC 72 carbon, (ii) CoTMPP, (iii) CoTMPP absorbed on carbon, (iv) at 410 °C, (v) at 440 °C, (vi) at 600 °C, (vii) at 700 °C, (viii) at 800 °C, (ix) at 810 °C. The instrument was calibrated using silicon wafer prior to each measurement. Aperture: 100×; laser power wavelength: 532 nm; power strength: 10%.

ferent sites on the surface of the carbon supporting material were measured to acquire a clear Raman signal of the catalyst. Vulcan carbon, since the material itself is fairly amorphous, only shows two weak bumps, located at 1323 and 1569 cm^{-1}, respectively, in the characteristic feature region of carbon (1200–1600 cm^{-1}). The spectrum for CoTMPP also lacks peaks, and instead, exhibits bumps centering at 1231 (weak), 1335 (weak), 1365, 1486 and 1551 cm^{-1}. These can generally be explained by the lack of intense polarity arising from the symmetric core of CoTMPP (Co with 4N's) leading to the Raman vibration modes (E, T and G) to be weak. Once the CoTMPP was absorbed on carbon and pyrolyzed, the active Raman peaks centering at 1348 (wide) and 1577 cm^{-1} appear (not all the sites measured exhibited this phenomenon), suggesting an interaction between large CoTMPP molecules and the carbon support. Generally, the bands characteristic of carbon materials are typically present at 1580 and 42 cm^{-1} [10], and the two peaks arising around 1350 and 1620 cm^{-1}, known as *D* and *D′* bands, respectively, are directly related to the edge plane of hexagonal carbon layers as well as some layer structural disorder [11]. These latter two peaks may shift somewhat or be a bit vague, and can even disappear on the different carbon materials. For the pyrolyzed CoTMPP/C samples used in this measurement, the *D* band is highly likely to correlate to a graphene structure (carbon layer structure), revealing that CoTMPP reacts with graphene via the organic solvent and pyrolysis. Among the pyrolyzed CoTMPP/C samples, the spectra of CoTMPP/C heated below 700 °C always show two peaks at 1345–53 and 1581–89 cm^{-1}. However, these peaks are reflected to be weak bumps in the spectra of the CoTMPP/C pyrolyzed at 700 °C and above, suggesting an increase of disorder in CoTMPP/C crystal structures and the weakening of interactions between CoTMPP and the graphene layers of the carbon support.

3.4. Electrochemical measurements

According to the literature reports [12–14], chelate-structured Co–N_x centers, bonded to graphene layers of carbon, played the role of active sites to generate high catalytic activity for the ORR. Since the amount of Co–N_x decreases with increasing pyrolysis temperatures and Co^{2+}/Co^{3+} oxide quantities, CoTMPP/C heat-treated at the beginning of the molecular structure change (Section 3.1) preserves the highest ORR catalytic activity. As a result, the main focus of the electrochemical measurements in this report is on the catalyst pyrolyzed at 410 °C, as it exhibits a number of promising attributes as a major catalyst in applicable alkaline fuel cells, and the catalyst pyrolyzed at 800 °C, as it is used by groups internationally in single cell tests due to its relatively good stability in acidic circumstances. LSV, CV and RRDE techniques were all used to characterize the ORR catalytic performances of CoTMPP/C pyrolyzed at the different temperatures.

The LSV plot, obtained by RRDE techniques, provides information on the catalytic activity of the evaluated catalyst, including the ORR onset potential and the mass transfer limiting current (the plateau current) of ORR. Fig. 4 shows the LSV plots obtained with CoTMPP/C catalysts pyrolyzed at various temperatures (410, 440, 600, 760, 800, and 810 °C), and the LSV plot with commercial Pt/C catalyst for comparison (the inset). It should be noted that, different from the commonly observed ORR LSV behavior in acidic solution, which features an initial increase in current followed by a steady value of the current (plateau current), the LSV plots of ORR in concentrated KOH (e.g., 6 M in this work) exhibit a peak current due to the diffusion limitation associated with the low solubility of oxygen in the 6 M KOH. Although utilizing much lower concentrations of KOH is a way of eliminating the peaks [15,16], it is in our interest to study the catalysts in concentrated alkaline solution, as it is more interesting from an application point of view.

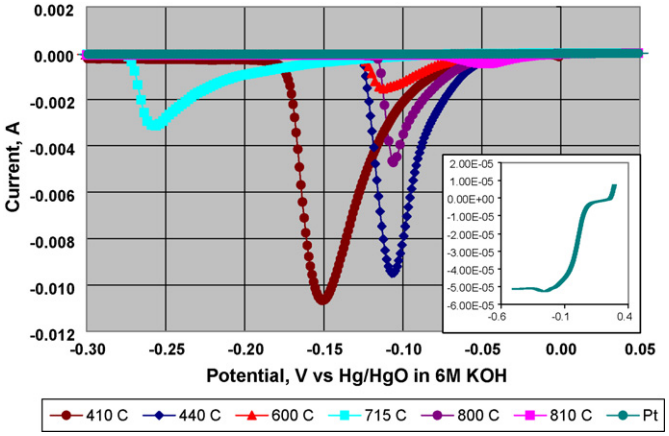

Fig. 4. Linear scanning voltammograms of the CoTMPP/C catalysts pyrolyzed at 410 °C, 440 °C, 600 °C, 700 °C, 800 °C, and 810 °C. The scanning rate was 5 mV s^{-1}; rotation rate was 1600 rpm; the electrolyte was 6 M KOH. Note: the current values of the CoTMPP catalysts were taken from the first peak that appeared in the CV curves and the Pt curve was buried in the background. Inset: Pt ORR performance in 6 M KOH.

LSV plots in Fig. 4 show that the ORR peaks of the CoTMPP/C catalysts pyrolyzed at lower temperatures (410 and 440 °C) are much bigger than those of the catalysts pyrolyzed at higher temperatures (800 and 810 °C), indicating that the CoTMPP/C pyrolyzed at the lower temperatures exhibited a much higher ORR limiting current. Interestingly, the peak currents of all the CoTMPP/C catalysts are at least one order of magnitude higher than Pt (inset of Fig. 4). In terms of the kinetics, at a fixed kinetic current (e.g., 0.001 A for most catalysts in Fig. 4), the catalyst pyrolyzed at 440 °C shows the most positive potential for ORR, followed by catalysts pyrolyzed at 800, 410, 600 and 715 °C. Considering both the peak current and the ORR potential, we concluded that catalysts pyrolyzed at lower temperatures (410 and 440 °C) exhibited a superior catalytic activity than those pyrolyzed at higher temperatures.

Stability tests, for the CoTMPP/C catalysts separately pyrolyzed at 410 and 800 °C, were conducted in concentrated alkaline solution by running CVs for 5000 cycles (Fig. 5a and b). The CoTMPP/C catalyst pyrolyzed at 410 °C showed a better performance than the catalyst pyrolyzed at 800 °C after 5000 cycles (Fig. 5c). The ORR peak currents of the 5000th cycle of both CoTMPP/C catalysts were higher than the values of Pt. It is also of interest that the capacities of both CoTMPP/C catalysts increased more than three times after 5000 cycles, which can be explicitly interpreted as the intercalation of ions; however, the identity of the foreign ions is still under investigation. This provides direct evidence that chelate-structured Co–N_x species have directly linked with the graphene layer, resulting in the opening of the graphene, allowing ease of access to foreign ions.

The electrochemical ORR mechanism for the CoTMPP/C catalysts, pyrolyzed at 410 and 800 °C, respectively, was studied using RRDE. Figs. 6 and 7 display the ring and disk currents for both CoTMPP/C samples at a rotating rate of 1600 rpm. The electron transfer number and percentage of H_2O_2 yielded were calculated based on the following equations [17,18]:

$$n = \frac{4I_d}{I_d + (I_r/N)} \quad (1)$$

$$\%H_2O_2 = \frac{100(2(I_r/N))}{I_d + (I_r/N)} \quad (2)$$

where *N* is the collection efficiency of the RRDE, I_d and I_r are the faradic currents at the disk and ring, respectively. Both calculated numbers have been summarized in Table 1. From the table, it is evident that the electron transfer number for ORR is different for

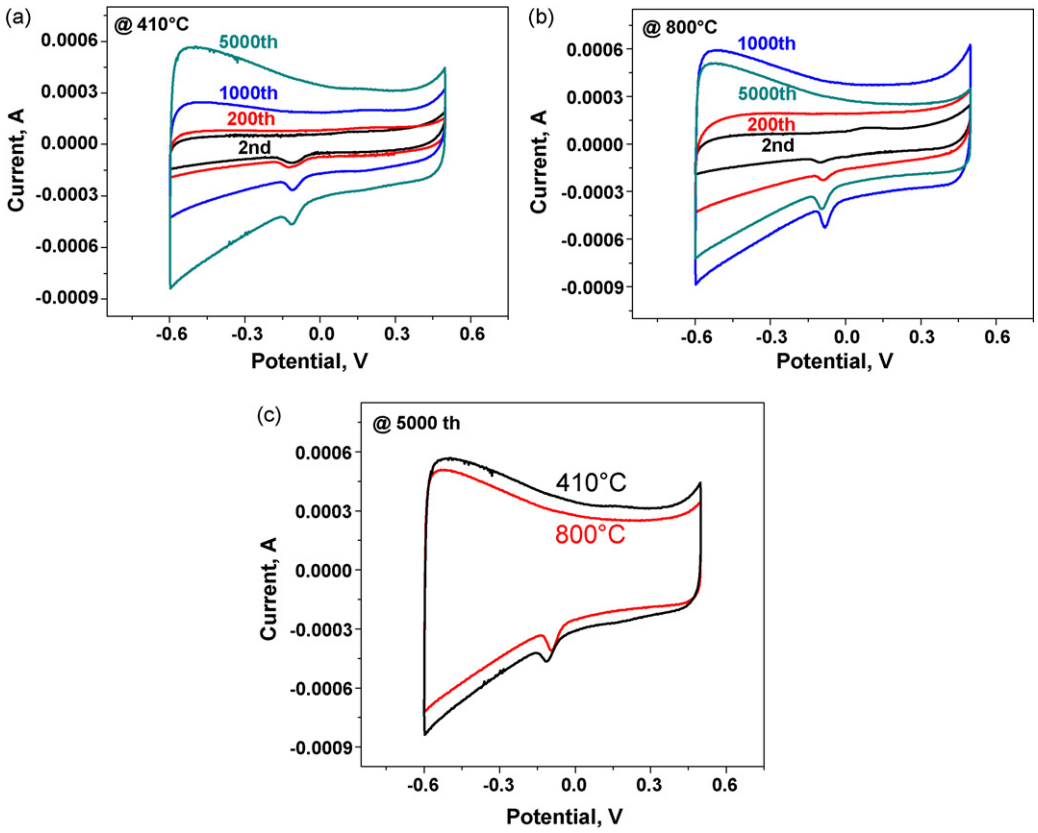

Fig. 5. Cyclic voltammograms of the 5000-cycle-durability tests for the COTMPP/C catalysts pyrolyzed at (a) 410 °C, and (b) 800 °C, with a scanning rate of 100 mV s^{-1} in 6 M KOH. Potential scan range is −0.6 to +0.5 V *vs.* Hg/HgO (0.060 V *vs.* NHE); (c) comparison between CoTMPP/C pyrolyzed at 410 and 800 °C after 5000 cycles.

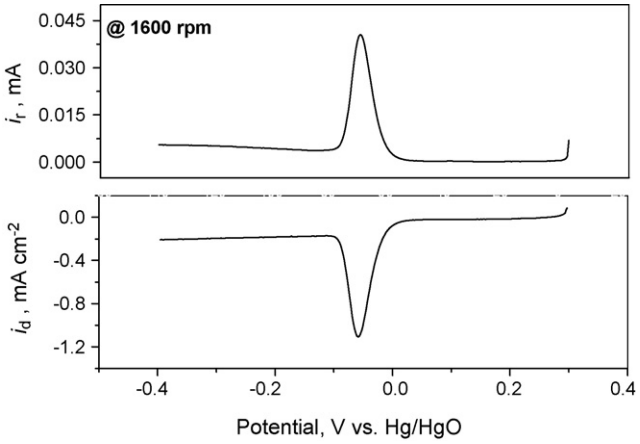

Fig. 6. Ring current (top) and disk current density (bottom) for the CoTMPP/C catalyst pyrolyzed at 410 °C with a potential scanning rate of 2 mV s^{-1} in 6 M KOH electrolyte. Rotating rate is 1600 rpm.

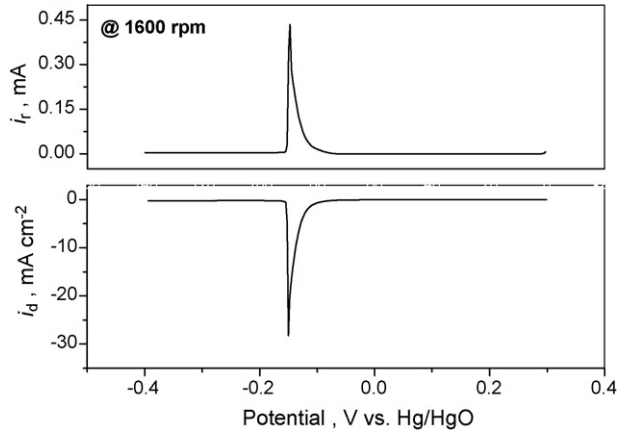

Fig. 7. Ring current (top) and disk current density (bottom) for the CoTMPP/C catalyst pyrolyzed at 800 °C with a potential scanning rate of 2 mV s^{-1} in 6 M KOH electrolyte. Rotating rate is 1600 rpm.

Table 1
Electron transfer number and the H_2O_2 yield of the CoTMPP/C catalysts pyrolyzed at 410 and 800 °C.

Cycle number	$n_{410\,°C}$	$n_{800\,°C}$	$H_2O_2\%_{410\,°C}$	$H_2O_2\%_{800\,°C}$
1	2.92	3.88	54.0	6.0
2	3.01	3.89	49.5	5.5
3	3.07	3.88	46.5	6.0
4	3.08	3.89	46.0	5.5
5	3.07	3.91	46.5	4.5
6	3.09	3.89	45.5	5.5

n: electron transfer number.

CoTMPP/C pyrolyzed at 410 and 800 °C, which are close to 3 and 4, respectively. Further, it can be seen from the table that, in general, the yield of H_2O_2 by CoTMPP/C pyrolyzed at 410 °C is higher than that of CoTMPP/C heat-treated at 800 °C, whereas the electron transfer number for ORR is lower. Therefore, for ORR, it is clear that the catalytic species of both catalysts pyrolyzed at the two different temperatures are not the same.

3.5. Single cell testing

To further compare the CoTMPP/C catalysts pyrolyzed at 410 and 800 °C, the two catalysts were tested in a home-designed unit cell

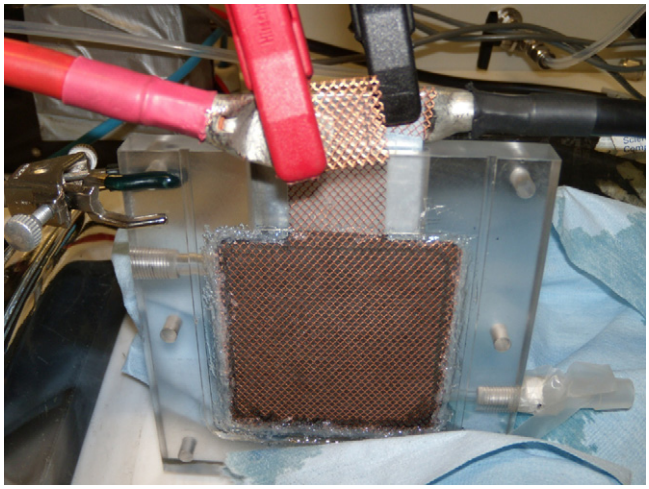

Fig. 8. Home-made single cell used for examining the catalyst performance in Zn-air fuel cell.

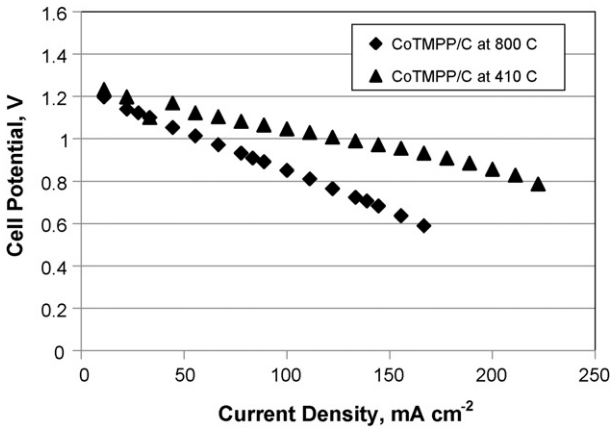

Fig. 9. Polarization curves of CoTMPP/C catalysts in single fuel cell test, CoTMPP/C pyrolyzed (a) at 410 °C and (b) at 800 °C.

shown in Fig. 8. The polarization curves representing the performance of the two catalysts in a single fuel cell test are illustrated in Fig. 9. The losses, due to the activation shown in both curves, are low. Although the catalyst loading for CoTMPP/C pyrolyzed at 410 °C is lower than that of CoTMPP/C pyrolyzed at 800 °C (0.08 *vs.* 0.09 mg cm^{-2}), its cell performance is still better than the latter, showing full consistency with the three-electrode cell electrochemical measurements shown above. Moreover, even with such a low catalyst loading, the current density was still able to reach 120 mA cm^{-2} at 1 V.

3.6. XPS, SAM, and TEM/BSE measurements

The electrode surface components are responsible for the ORR and the electrochemical effective depth on the solid side of the liquid/solid interface is in the range of a few angstroms to a few

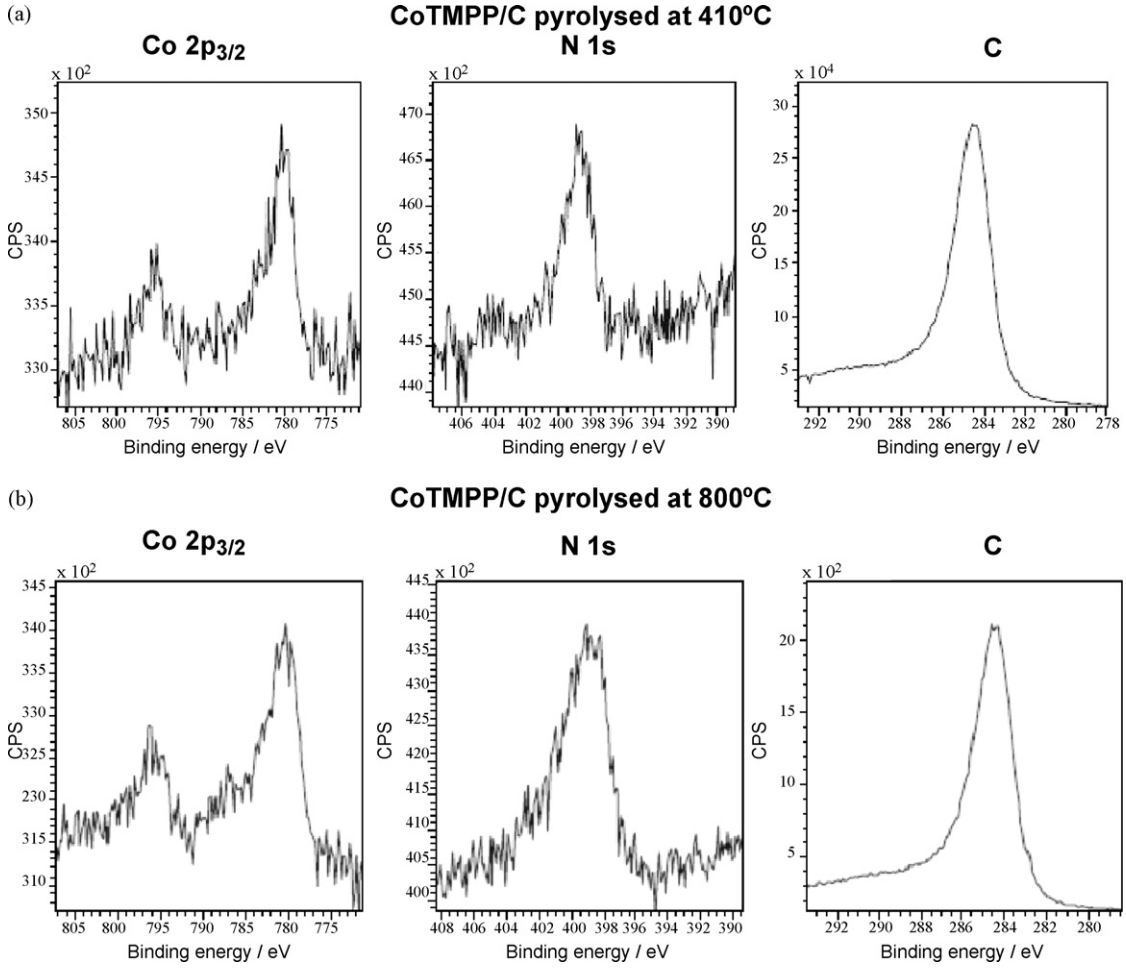

Fig. 10. XPS spectra of CoTMPP/C pyrolyzed at (a) 410 °C and (b) 800 °C.

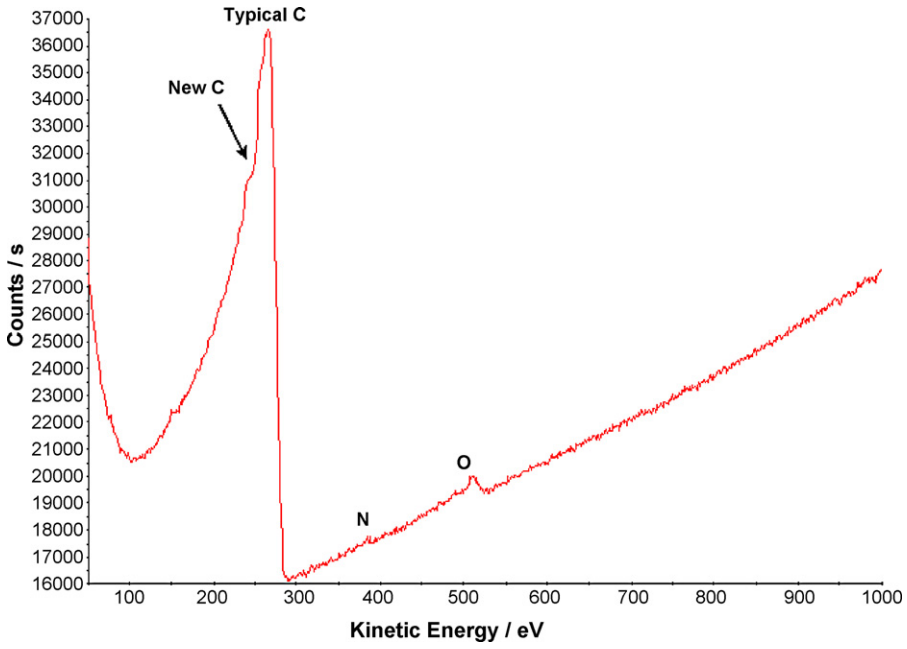

Fig. 11. SAM high-resolution spectrum of the newly appeared chemical bond in the absence of Co.

nano-meters. Since XRD can only access a depth of a few micrometers, XPS was used to measure the presence of Co–N_x segments at the electrode surfaces of CoTMPP/C pyrolyzed at 410 and 800 °C, respectively. To achieve reproducible results with high-spectrum resolution for the two independent trials, XPS measurements were performed twice on each of the four catalyst samples used in the two repeatable electrochemical experiment sets. The results of the measurements are shown in Fig. 10a and b. The binding energies (BE) of Co $2p_{3/2}$ for the catalysts pyrolyzed at 410 and 800 °C were found to be consistently located between 780.18 and 780.40 eV, demonstrating the association of Co^{2+} with varying organic moieties for both catalysts [19]. However, the difference between the BE of Co for the two catalysts, pyrolyzed at the different temperatures, is negligible, suggesting that the difference in catalytic activity between the two catalysts may not stem from the change of Co chemical state. The BE of N 1s of the sample pyrolyzed at 410 °C is around 398.46 eV, while it is about 398.81 eV for the catalyst pyrolyzed at 800 °C, indicating that the Co–N bonding in the catalyst pyrolyzed at 800 °C is stronger than that in the catalyst pyrolyzed at 410 °C. The carbon chemical states of the catalysts are difficult to demarcate due to the influence of the adventitious carbon. Regarding the Co/N ratio, measured by XPS, it can be seen that for the CoTMPP/C sample pyrolyzed at 410 °C, the Co/N ratio of the catalyst is always lower than that of the CoTMPP/C pyrolyzed at 800 °C (1:4.7 *vs.* 1:5.9). This indicates that the CoTMPP/C, pyrolyzed at 410 °C, has more organic moieties to bond chemically and the

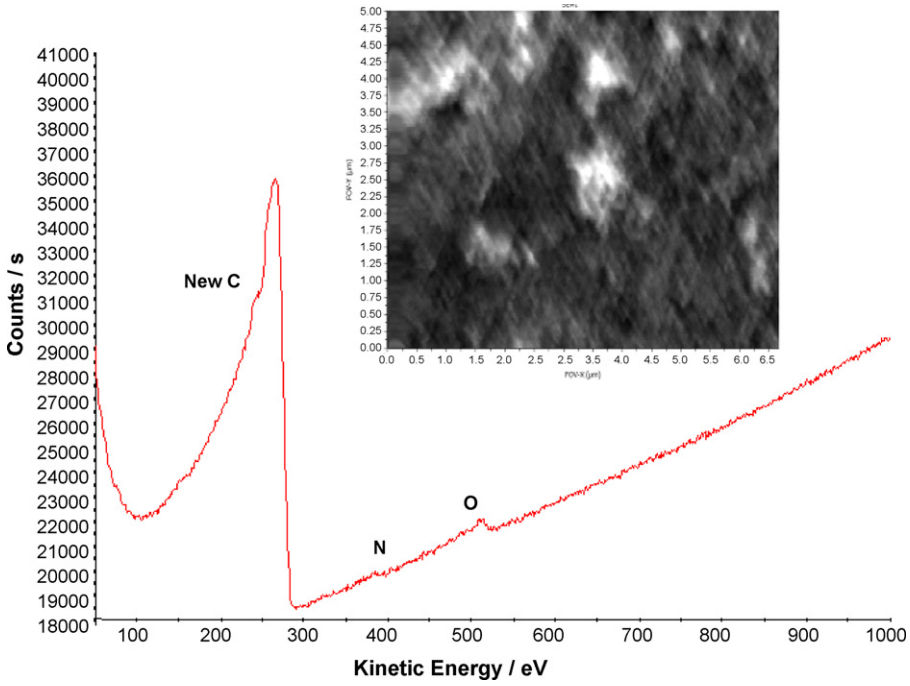

Fig. 12. BSE image combined with SAM survey for presenting the distribution of the catalytic active sites containing only N, C and O.

major catalytic components for the samples treated respectively at 410 and 800 °C are different yielding the different electron transfer numbers for ORR. A general thought about the catalytic structure of CoTMPP for ORR is that it is built based on the chelate structure, i.e., the core structure of CoTMPP (Co with 4N or 2N). If so, Co–N would play a major role in accelerating electron transfer during ORR and its chemical bonding state would show a slight difference for different CoTMPP/C catalysts unless CoTMPP/C was pyrolyzed at very high temperatures, resulting in a complete decomposition of the chelate structure. The XPS results obtained in this work support this viewpoint, showing a marginal difference of the Co–N binding energies of the catalysts pyrolyzed at 410 and 800 °C, respectively.

SAM was also employed to investigate the catalytic components of CoTMPP/C, and interestingly, the several reproducible SAM spectra for the measured surface areas of the catalyst pyrolyzed at 410 °C show a shoulder representing a new C bond coordinated only with N and/or O (Fig. 11). In this case Co is totally absent, eliminating it from the catalytic moiety. This result coincides with the Raman result which shows the *D* and *D′* bands of carbon are activated (Section 3.3). It is worth noting that this shoulder was not found in the sample pyrolyzed at 800 °C, additionally confirming the XPS results that the major catalytic components differ between the two catalysts pyrolyzed at two temperatures.

In a further effort to clarify the results from SAM, high-resolution TEM and back scattering electron imaging (BSE) were performed in conjunction with the Auger scanning survey. It can be seen in Fig. 12 that the catalyst surface sites, which contain only N, C and O, are randomly distributed, however, no segregation or severe agglomeration of particles was found. Further to the SAM results, high-resolution TEM micrographs showed that, among the large amount of carbon grain overlapping, there were Co clusters, as marked in red. Furthermore, the local EDX clearly indicates these

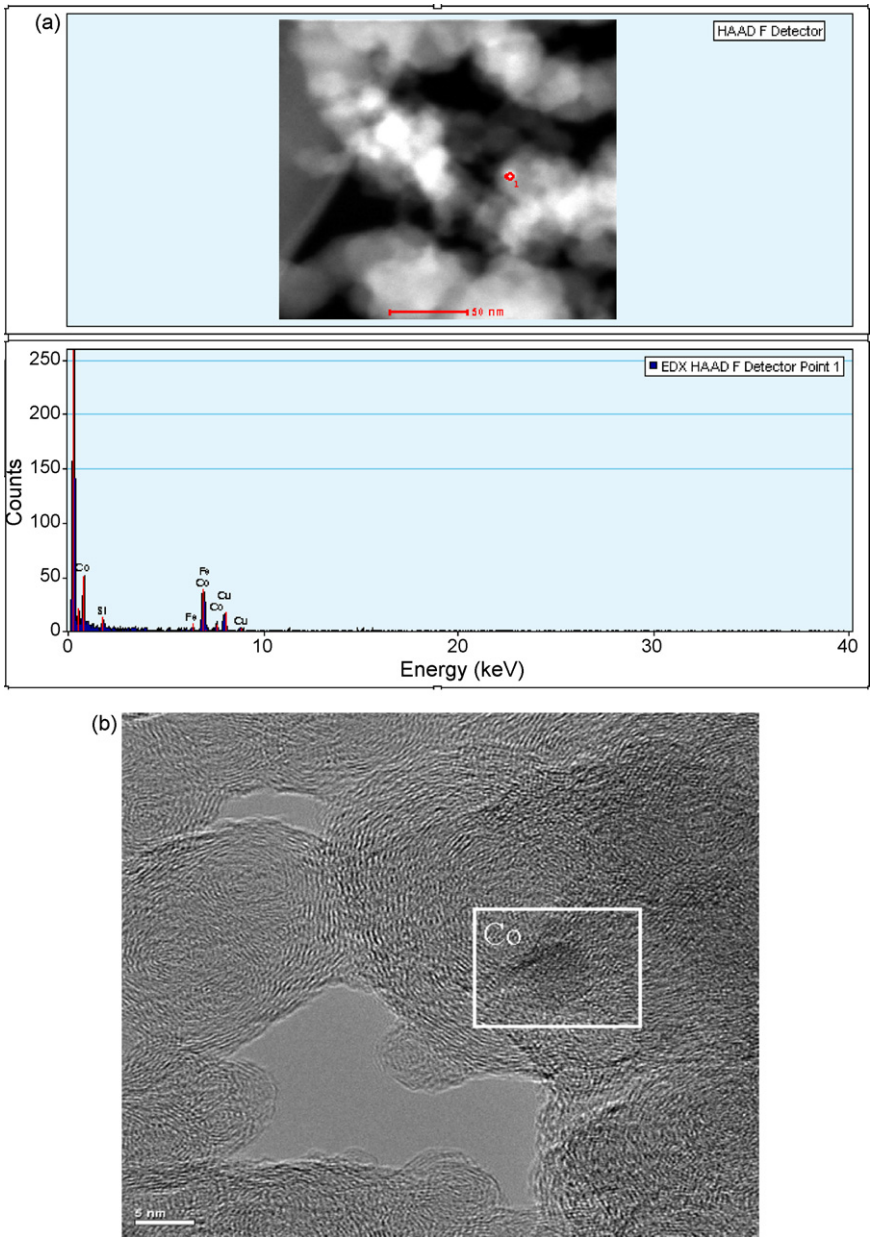

Fig. 13. High-resolution TEM image of Co nanocrystal with local EDAX spectrum (a) and details of Co on carbon matrix (b). Note that in EDAX spectrum the appearance of Cu is due to the grid of the TEM sample holder, Si is an impurity coming from the ceramic boat used for the CoTMPP sample heat treatment at high temperature and Fe should be Co since the β1 and β2 lines between Fe and Co are very close, resulting in a difficulty in distinguishing Co and Fe when auto-identification is performed by TEM EDX analyzer.

tiny clusters are Co nanocrystals (Fig. 13a). The 5 nm scale resolution image, Fig. 13b, further revealed that Co was trapped within the carbon matrix making it absent from the SAM, as well as difficult to discern within the TEM image. It can be seen from the fringe print pattern of Fig. 13b that Co nanocrystals may react somewhat with the carbon matrix, but the integration level is low. Since it is the surface of the catalyst that has been proven to be catalytically active by electrochemical examinations (see Section 3.4), and it is known that CoTMPP/C, when pyrolyzed at 410 °C, is more catalytically active than the catalyst pyrolyzed at 800 °C, it can only be deduced that there is a N–C(O) moiety that possesses catalytic properties. Furthermore, it can also be derived that this catalytic segment of CoTMPP/C is further decomposed at high temperatures, such as 800 °C. Very recently, Gong et al. [15] have reported that a tightly packed and vertically aligned carbon nanotubes doped with N atoms have superior ORR performance than Pt in 0.1 M KOH alkaline electrolyte. It seems there is an undisclosed link between N–C reactivity in this case and in ours; however, how the C is activated during the pyrolysis processes and what the genuine structure of N–C(O) that catalyzes O is, still requires further investigation.

4. Concluding remarks

As a potential candidate for use in alkaline fuel cells and metal–air batteries, CoTMPP/C catalysts, pyrolyzed at varying temperatures, were studied and compared to determine the effect of pyrolysis temperature on the catalytic activity. Electrochemical evaluation conducted using CV, LSV, and RDE techniques in a three-electrode cell revealed that a low catalyst loading (about 3–5 wt%) of CoTMPP yielded an order-of-magnitude higher current towards the ORR when compared with Pt at the same loadings in concentrated alkaline electrolyte (pH > 14); in addition, the electrochemical measurements have also shown that CoTMPP/C pyrolyzed at 410 °C has higher catalytic activities than the catalyst pyrolyzed at 800 °C. Furthermore, for the low temperature pyrolysis, the electron transfer number for ORR, as well as the namely core catalytic Co–N moiety, are different from those of CoTMPP/C heat-treated at 800 °C, which is the main-stream catalyst in literatures concerning CoTMPP applications. Moreover, although CoTMPP/C, pyrolyzed at 410 °C, was shown, by RRDE, to generate a higher current for ORR, it also exhibited a higher H_2O_2 yield as compared with CoTMPP/C pyrolyzed at 800 °C. Both CoTMPP/C catalysts (pyrolyzed at 410 and 800 °C) were seen to endure 5000 cycles in durability tests via the CV method.

The single fuel cell testing also indicated that CoTMPP/C pyrolyzed at 410 °C had a better performance than CoTMPP/C pyrolyzed at 800 °C, which is fully consistent with the results obtained from electrochemical examination conducted in the three-electrode cell. Although the current density was shown to reach a value above 120 mA cm^{-2} at 1 V with the very low catalyst loading of 0.08 mg cm^{-2} in the single cell testing, it is suggested that the catalyst loading be increased to a relatively higher level, e.g., 0.6 mg cm^{-2} (Pt loading level), for applications in the future.

Raman, in conjunction with XRD analysis, has shown that strong interaction between CoTMPP and Vulcan carbon support occurs during the pyrolysis processes. Additionally, the appearance of a new D-band, observed near 1350 cm^{-1}, in the Raman spectra indicates that CoTMPP activates graphene and results in some graphene layers playing a vital role in oxygen reduction catalysis. Moreover, SAM, in conjunction with TEM/BSE, have revealed a new N–C(O) bond in CoTMPP/C catalyst pyrolyzed at 410 °C, which is believed to contribute to its superior performance as a catalyst when compared to the industry standard of pyrolysis at 800 °C.

Acknowledgments

The authors would like to thank Dr. K. Wang and Dr. P. Wong at the University of British Columbia for their support in XPS and SAM analysis.

References

[1] F. Bidault, D.J.L. Brett, P.H. Middleton, N.P. Brandon, J. Power Sources 187 (2009) 39–48.
[2] O. Haas, F. Holzer, K. Müller, S. Müller, in: W. Vielstich, H.A. Gasteiger, A. Lamn (Eds.), Handbook of Fuel Cells—Fundamentals, Technology and Applications, vol. 1, John Wiley, 2003 (Chapter 22).
[3] H.A. Gasteiger, S. Kocha, B. Sompalli, F.T. Wagner, Appl. Catal. B 56 (2005) 9–35.
[4] M. Lefèvre, E. Proietti, F. Jaouen, J.P. Dodelet, Science 324 (2009) 71–74.
[5] J.J. Zhang (Ed.), PEM Fuel Cell Electrocatalysts and Catalyst Layers: Fundamentals and Applications, Springer, 2008.
[6] T.J. Schmit, H.A. Gasteiger, G.D. Stäb, P.M. Urban, D.M. Kolb, R.J. Behm, J. Electrochem. Soc. 145 (1998) 2354–2358.
[7] U.A. Paulus, T.J. Schmidt, H.A. Gasteiger, R.J. Behm, J. Electroanal. Chem. 495 (2001) 134–145.
[8] U.I. Herrmann, S. Kramm, P. Fiechter, Bogdanoff, Electrochim. Acta 54 (2009) 4275–4287.
[9] B.D. Cullity, S.R. Stock, Elements of X-ray Diffraction, 3rd edition, Addison-Wesley, Boston, MA, 1998.
[10] A.K. Gupta, T.J. Russin, H.R. Gutiérrez, P.C. Eklund, ACS Nano 3 (2009) 45–52.
[11] M. Inagaki, F.Y. Kang, Carbon Materials Science and Engineering—From Fundamentals to Applications, Tsinghua University Press, 2006, p. 119.
[12] D.A. Scherson, A. Tanaka, S.L. Gupta, D. Tryk, C. Fierro, R. Holze, E.B. Yeager, Electrochim. Acta 31 (1986) 1247–1258.
[13] M. Lefèvre, J.P. Dodelet, P. Bertrand, J. Phys. Chem. B 104 (2000) 11238–11247.
[14] G. Faubert, G. Lalande, R. Côte, D. Guay, J.P. Dodelet, L.T. Weng, P. Bertrand, G. Dénès, Electrochim. Acta 41 (1996) 1689–1701.
[15] K. Gong, F. Du, Z.H. Xia, M. Durstock, L.M. Dai, Science 323 (2009) 760–764.
[16] T.C. Nagaiah, S. Kundu, M. Bron, M. Muhler, W. Schuhmann, Electrochem. Commun. 12 (2010) 338–341.
[17] X.Y. Xie, Z.F. Ma, X.X. Ma, Q.Z. Ren, V.M. Schmidt, L. Huang, J. Electrochem. Soc. 154 (8) (2007) B733–B738.
[18] X.Y. Xie, Z. FMa, X. Wu, Q.Z. Ren, X.X. Yuan, Q.Z. Jiang, L.Q. Hu, Electrochim. Acta 52 (2007) 2091–2096.
[19] J.F. Moulder, W.F. Stickle, P.E. Sobol, K.D. Bomben, in: J. Chastain, R.C. King Jr. (Eds.), Handbook of XPS, Physical Electronic Inc., 2003.